We are IntechOpen,
the world's leading publisher of
Open Access books
Built by scientists, for scientists

6,900
Open access books available

186,000
International authors and editors

200M
Downloads

154
Countries delivered to

Our authors are among the

TOP 1%
most cited scientists

12.2%
Contributors from top 500 universities

BOOK CITATION INDEX
CLARIVATE ANALYTICS
INDEXED

WEB OF SCIENCE™

Selection of our books indexed in the Book Citation Index
in Web of Science™ Core Collection (BKCI)

Interested in publishing with us?
Contact book.department@intechopen.com

Numbers displayed above are based on latest data collected.
For more information visit www.intechopen.com

Nonlinear and Sampled Data Control of Wind Turbine

Marwa Hassan

Abstract

This chapter aims to investigate the effectiveness of the nonlinear control-based model and the sampled-data design through the power system application. In particular, the study will focus on a model of a wind turbine system fed by a doubly fed induction generator (DFIG). First of all, a detail dynamical model of a DFIG-based wind-turbine grid-connected system is presented in the direct and quadratic synchronous reference frame. Afterward, mathematical modeling is performed for the nonlinear and sampled data systems. The nonlinear control will ensure the reproduction of the rotor direct and quadratic current that converge to the reference signal generated from. The proposed sampled-data system is built upon the nonlinear model and is introduced as an alternative of the classical discrete control which is known as emulation design. The simulation's results will show that implementing the approximate feedback will yield better results than the one obtained from the mere emulation.

Keywords: sampled data model, nonlinear control, renewable energy, wind turbine, feedback

1. Introduction

In recent years global warming emissions have been one of the most important topics discussed by the researcher. The carbon dioxide causes harmful impacts on the environment as it acts like a blanket that traps heat. According to the latest survey done in the United States, about 29% of global warming emissions are caused by fossil fuel used in the electricity sector [1–3]. Therefore it becomes more essential to look for alternative sources. Renewable energy sources especially wind energy produce little to no global warming emissions as burning natural gas for electricity releases between 0.6 and 2 pounds of carbon dioxide equivalent per kilowatt-hour (CO_2E/kWh); coal emits between 1.4 and 3.6 pounds of CO_2E/kWh. Wind, on the other hand, is responsible for only 0.02–0.04 pounds of CO_2E/kWh on a life-cycle basis [3]. In conclusion, Wind energy represents one of the fastest-growing energy sources in the world due to it is a major advantage in terms of cost and effectiveness [4–8]. The wind farm system based on the doubly fed induction generator (DFIG) will be studied in this chapter. In simple words, the DFIG is a generator that has its rotor winding connected to the grid via slip rings and back-to-back voltage source converters that control both the rotor and the grid currents. Thus, rotor frequency can freely differ from the grid frequency. DFIG has become more effective in the industry in the last few years due to its advantage compared to

the permanent magnet synchronous generator as it provides better results when compared to cost, size, and weight. A lot of researches have been carried out in the area of modeling and controlling of stator/rotor flux in DFIG [9–11]. Most of these researches face some drawbacks due to the nonlinear nature of the DFIG. Examples can be found on [12–19]. In this chapter, we aim to introduce a nonlinear control technique that aims to reproduce an output signal that converges to a distinct reference signal. Later on, the sampled data control technique will be applied as an alternative solution of the emulation based technique that is usually applied to the nonlinear system. A few examples of the sampled data are illustrated in [20–22]. The chapter is structured as follow: Section 2 recalls the modeling considerations of the doubly fed induction generator while Section 3 illustrates the nonlinear control approach. Section 4 presents the Grid side command model. Finally, Section 5 presents the sampled data model and the obtained results while Section 6 concludes the paper and formulates further research directions.

2. Modeling

The modeling of the doubly fed induction generator (DFIG) will be recalled in this section. These equations will be used to design the nonlinear control system.

2.1 Doubly fed induction generator model

1. Stator equations

$$V_{sd} = R_s i_{sd} + \frac{d}{dt}\lambda_{sd} - \lambda_{sq}W_s \tag{1}$$

$$V_{sq} = R_s i_{sq} + \frac{d}{dt}\lambda_{sq} + \lambda_{sd}W_s \tag{2}$$

$$\lambda_{sd} = L_s i_{sd} + M i_{rd} \tag{3}$$

$$\lambda_{sq} = L_s i_{sq} + M i_{rq} \tag{4}$$

2. Rotor equations

$$V_{rd} = R_r i_{rd} + \frac{d}{dt}\lambda_{rd} - \phi_{rq}W_r \tag{5}$$

$$V_{rq} = R_r i_{rq} + \frac{d}{dt}\lambda_{rq} + \phi_{rd}W_r \tag{6}$$

$$\lambda_{rd} = L_r i_{rd} + M i_{sd} \tag{7}$$

$$\lambda_{rq} = L_r i_{rq} + M i_{sq} \tag{8}$$

$$W_r = g.W_s \tag{9}$$

with

$$i_{sd} = \frac{\lambda_{sd} - M i_r d}{L_s} \tag{10}$$

$$i_{sq} = \frac{-M i_{rq}}{L_s} \tag{11}$$

where R_s and R_r are, respectively, the stator and rotor phase resistances, Ls, Lr, M Stator and rotor per phase winding and magnetizing inductances and W_s, W_r are the stator and rotor speed pair pole number. The direct and quadrate stator and rotor currents are respectively represented as i_{sd}, i_{sq}, i_{rd} and i_{rq}. The electromagnetic torque is presented by the following equation:

$$J\frac{dW_r}{dt} + f_r W_r = c_{em} - c_r \tag{12}$$

$$C_{em} = p\left(\lambda_{rq}i_{rd} - \lambda_{rd}i_{rq}\right) \tag{13}$$

The system now will be modeled with respect to the rotor side direct and quadratic (d, q) synchronous reference frame. The input in such case are I_{rd} and I_{rq}. First the system expression w.r.t d axis frame:

$$v_{rd} = R_r i_{rd} + \frac{d}{dt}(L_r i_{rd} + M i_{sd}) - (L_r i_{rq} + M i_{sq})W_r \tag{14}$$

$$= R_r i_{rd} + \frac{d}{dt}i_{rd}\left(L_r - \frac{M^2}{L_s}\right) - L_r i_{rq}W_r - MW_r\left(\frac{-M i_{rq}}{L_s}\right) \tag{15}$$

$$R_r i_{rd} + L_r \frac{d}{dt}i_{rd}\left(1 - \frac{M^2}{L_s L_r}\right) - L_r i_{rq}W_r + \frac{M^2}{L_s}W_r i_{rq} \tag{16}$$

$$= R_r i_{rd} + L_r \dot{i}_{rd}\left(1 - \frac{M^2}{L_s L_r}\right) - L_r W_r\left(1 - \frac{M^2}{L_s L_r}\right)i_{rq} \tag{17}$$

$$= R_r i_{rd} + L_r \Lambda \dot{i}_{rd} - L_r \Lambda W_r i_{rq} \tag{18}$$

$$\dot{i}_{rd} = \frac{1}{L_r \Lambda}v_{rd} - \frac{R_r}{L_r \Lambda}i_{rd} + w_r i_{rq} \tag{19}$$

$$\dot{i}_{rd} = \frac{1}{L_r \Lambda}v_{rd} - \frac{1}{\mathcal{T}\Lambda}i_{rd} + w_r i_{rq} \tag{20}$$

with $\Lambda = \left(1 - \frac{M^2}{L_s L_r}\right) \mathcal{T} = \frac{R_r}{L_r}$.

Now consider q axis frame:

$$V_{rq} = R_r i_{rq} + \frac{d}{dt}\lambda_{rq} + \lambda_{rd}W_r \tag{21}$$

$$= R_r i_{rq} + \frac{d}{dt}\left(L_r i_{rq} - \frac{M^2}{L_s}i_{rq}\right) + W_r\left(L_r i_{rd} - \frac{M^2 i_{rd}}{L_S}\right) \tag{22}$$

$$= R_r i_{rq} + L_r \dot{i}_{rq}\left(1 - \frac{M^2}{L_s L_r} + L_r W_r\left(1 - \frac{M^2}{L_s L_r}\right)i_{rd} \tag{23}$$

$$= R_r i_{rq} + L_r \Lambda \dot{i}_{rq} - L_r \Lambda W_r i_{rd} \tag{24}$$

$$\dot{i}_{rq} = \frac{1}{L_r \Lambda}v_{rq} - \frac{1}{\mathcal{T}\Lambda}i_{rq} - w_r i_{rd} \tag{25}$$

Finally we obtain the speed from the torque equation as:

$$\dot{W}_r = -\frac{f_r}{J}W_r + \frac{p}{J}\lambda_{rq}i_{rd} - \frac{p}{J}\lambda_{rd}i_{rq} \tag{26}$$

3. Nonlinear control of the DFIG

First, we start by putting the model in the standard nonlinear form. Recalling from modeling, the system is introduced in the condensed nonlinear form:

$$\Sigma_C : \begin{cases} \dot{x} = f(x) + g_1(x)u_1 + g_2(x)u_2, & x \in \mathbb{R}^n, u \in \mathbb{R}^n \\ y = h(x). \end{cases} \tag{27}$$

where, $X = \begin{bmatrix} x_1 & x_2 & x_3 \end{bmatrix}^T = \begin{bmatrix} i_{rd} & i_{rq} & W_r \end{bmatrix}^T$, $U = \begin{bmatrix} u_1 & u_2 \end{bmatrix}^T = \begin{bmatrix} v_{rd} & v_{rq} \end{bmatrix}^T$. The function $f(x), g(x)$ are smooth vector fields and the output function $h(x)$ is a smooth scalar function.

$$f(x) = \begin{pmatrix} -\dfrac{1}{\mathscr{T}\Lambda}x_1 + x_2 x_3 \\ -\dfrac{1}{\mathscr{T}\Lambda}x_2 - x_2 x_3 \\ -\dfrac{f_r}{J}x_3 + \dfrac{p}{J}\phi_{rq}x_1 - \dfrac{p}{J}\phi_{rd}x_2 \end{pmatrix} \tag{28}$$

$$g_1(x) = \begin{pmatrix} \dfrac{1}{\mathscr{T}\Lambda} \\ 0 \\ 0 \end{pmatrix}, \quad g_2(x) = \begin{pmatrix} 0 \\ \dfrac{1}{\mathscr{T}\Lambda} \\ 0 \end{pmatrix}. \tag{29}$$

Since the purpose of this study is to control the rotor side converter current, the output was chosen as $h(x) = \begin{bmatrix} i_{rd}, i_{rq} \end{bmatrix}^T$.

Remark 1. *According to the previous results obtained by Isidori, A multi variable nonlinear system in the form of (36) has a relative degree $r_1, \ldots, r_m$ at point x^0 if $L_{g_j}L_f^k h_i(x) = 0$ for all $1 \leqslant j \leqslant m$, for all $1 \leqslant i \leqslant m$, for all $k \leqslant r_i - 1$, and for all neighbor of x^0.*

Following the same definition, it can be easily verified that the system relative degree w.r.t the outputs $r = 2$.

3.1 Control of d-axis rotor current

In order to track rotor current $i_r q$ we assume that the system is only affected by u_1 and $u_2 = 0$.

$$\dot{x} = f(x) + g_1(x) \tag{30}$$

$$y = h_1(x) = i_{rd} \tag{31}$$

The system relative degree w.r.t the output $r = 1$. Now we apply a coordinate transformation and introduce the system in to the normal form.

$$\phi(x) = \begin{pmatrix} z_1 = x_1 \\ \eta_1 = x_2 \\ \eta_2 = x_3, L_g.\eta = 0. \end{pmatrix} \tag{32}$$

4

$$\begin{cases} \dot{z}_1 = -\dfrac{1}{\mathscr{T}\Lambda}z_1 + \eta_1\eta_2 + \dfrac{1}{\mathscr{T}\Lambda}u_1 \\[2mm] \dot{\eta}_1 = -\dfrac{1}{\mathscr{T}\Lambda}\eta_1 - z_1\eta_2 \\[2mm] \dot{\eta}_2 = p\phi_{rd}z_1 - p\phi_{rd}\eta_1 - \dfrac{f_r}{J}eta_2 \end{cases} \tag{33}$$

After applying the proper control law in the form of $u = \mathscr{T}\Lambda\left(-\frac{1}{\mathscr{T}\Lambda}x_1 + x_2x_3 + x_1^r - c_0x_1\right)$ where x_1^r, c_0 represents the rotor current desired value and the chosen zero, we obtain the desired output.

3.2 Control of q-axis rotor current

In this case the effect of u_2 is studied

$$f(x) = \begin{pmatrix} -\dfrac{1}{\mathscr{T}\Lambda}x_1 + x_2x_3 \\[2mm] -\dfrac{1}{\mathscr{T}\Lambda}x_2 - x_2x_3 \\[2mm] -\dfrac{f_r}{J}x_3 + \dfrac{p}{J}\phi_{rq}x_1 - \dfrac{p}{J}\phi_{rd}x_2 \end{pmatrix} g_2(x) = \begin{pmatrix} 0 \\[2mm] \dfrac{1}{\mathscr{T}\Lambda} \\[2mm] 0 \end{pmatrix} \tag{34}$$

$$y = h_2(x) = i_{rq}. \tag{35}$$

The system relative degree $r_q = 1$. The coordinate transformation and the normal take the form of

$$\phi(x) = \begin{pmatrix} z_1 = x_2 \\ \eta_1 = x_3 \\ \eta_2 = x_1 \end{pmatrix} \tag{36}$$

$$\begin{cases} \dot{z}_1 = -\dfrac{1}{\mathscr{T}\Lambda}z_1 + \eta_1\eta_2 + \dfrac{1}{\mathscr{T}\Lambda}u_2 \\[2mm] \dot{\eta}_1 = p\phi_{rd}\eta_1 - p\phi_{rd}z_1 - \dfrac{f_r}{J}\eta_1 \\[2mm] \dot{\eta}_2 = -\dfrac{1}{\mathscr{T}\Lambda}\eta_2 - z_1\eta_2. \end{cases} \tag{37}$$

The input

$$u = \mathscr{T}\Lambda\left(-\dfrac{1}{\mathscr{T}\Lambda}x_2 - x_1x_3 + x_2^r - c_0x_2\right). \tag{38}$$

3.3 Simulation and results

This section presents the evaluation of the performance of the proposed technique. Two cases were developed. The first case study based on the Doubly Fed Induction Generator model while the second one studies the gird side converter command model when the power factor is set to unity. **Table 1** presents the parameters of the DIFG parameters. The Bitz limit at which the maximum efficiency is obtained for the first case study is shown in **Figure 1**. In this case, the optimal point corresponds to Beta angle is equal to zero. Two feedbacks were

The DFIG data of a typical 3.6 MW generator	
Power	7 kW
Efficiency at rated speed	79%
Voltage	690 V
Locked rotor voltage	1000 V
Operation speed range	2000 rpm
Power factor	0.90 cap
Rotor Resistance	1 Ω
Rotor Inductance	0.2 mH
Stator Resistance	0.5 Ω
Stator Inductance	0.001 mH
Mutual inductance	0.078 H
Number of poles	4
Inertia moment	0.3125 Nms^2

Table 1.
The DFIG data sheet.
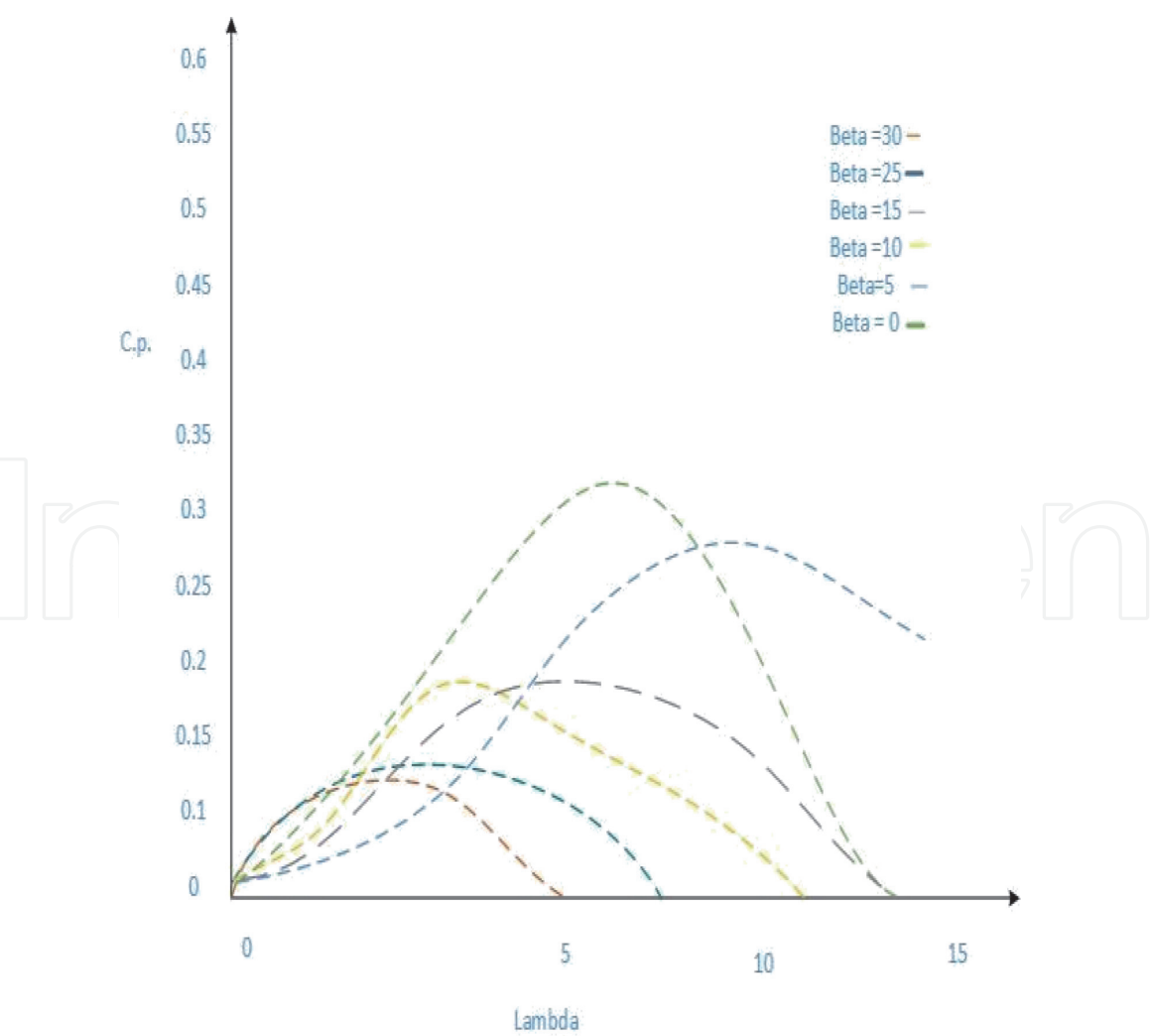
Figure 1.
Power coefficient curve.

applied in this stage in the sake of evaluating proposed control strategy. The primary feedback was applied in the direct axis frame with an input value

$$u = \mathscr{T}\Lambda\left(-\frac{1}{\mathscr{T}\Lambda}x_1 + x_2x_3 + x_1^r - 1000x_1\right) \tag{39}$$

Figure 2 shows the result of the rotor side reference signal and the generated current signals after applying the feedback. It can be noticed that the proposed control technique succeeded in reproducing a current signal that coincides with the required reference signal. As for the quadratic axis frame another feedback was designed to track the required current signal.

$$u = \mathscr{T}\Lambda\left(-\frac{1}{\mathscr{T}\Lambda}x_2 - x_1x_3 + x_2^r - 1200x_2\right) \tag{40}$$

The applied input will produce a signal that follows the reference signal (see **Figure 3**). **Figure 4** presents the continuous bus voltage of the DFIG regulated to the standard reference voltage fixed at 1000 V. It is clear that in spite of fluctuation of the wind the voltage remains stationary which is considered a major advantage as the system will be affected by the harmonics.

In the next half of this chapter, the sampled data design techniques and its application will be discussed. For the simplicity of the design, we choose to set the power factor to unity such that the system is converted to a SISO system. In such a case the Grid Side Converter command model is studied.
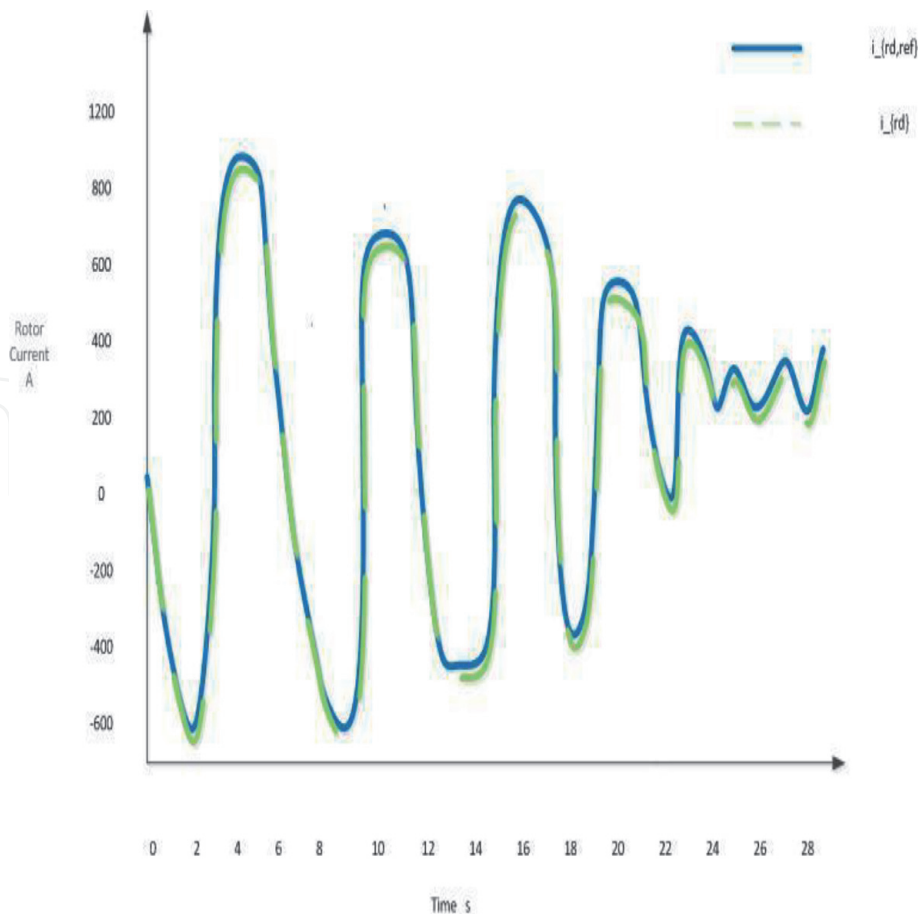

Figure 2.
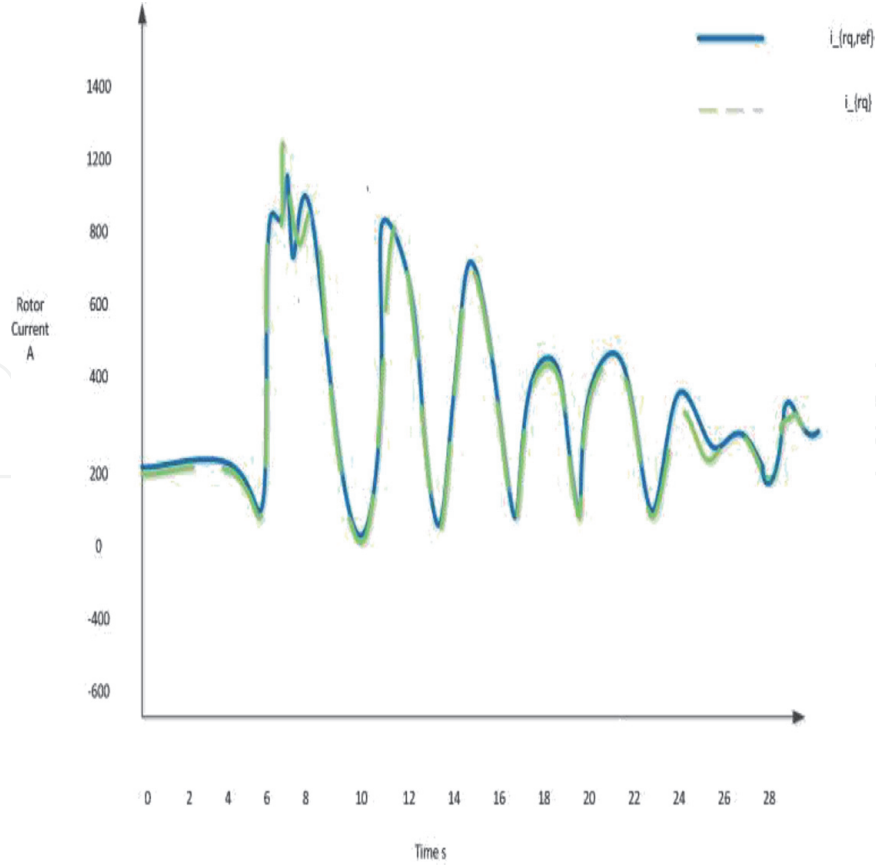*Doubly fed induction generator i_{rd} rotor current.*

Figure 3.
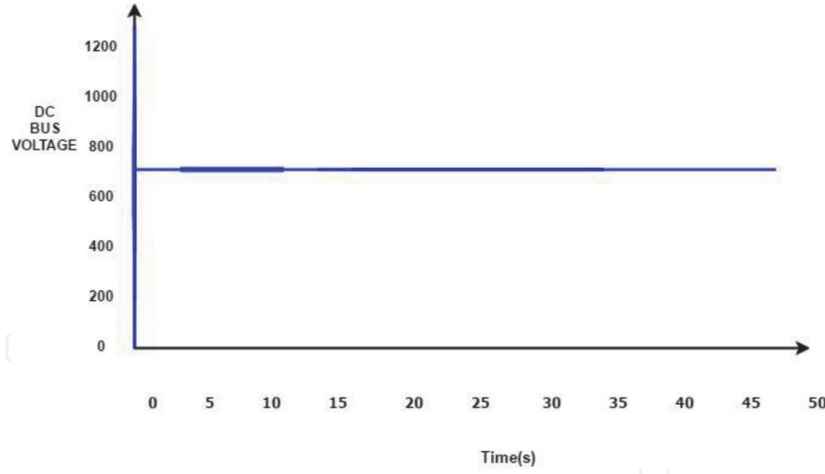*Doubly fed induction generator i_{rq} rotor current.*

Figure 4.
Doubly fed induction generator continuous bus voltage.

4. Grid side converter command model

$$v_{fd} = R_f i_{fd} + L_f \frac{d}{dt} i_{fd} - W_r L_f i_{fq} - V_{Gd} \tag{41}$$

$$v_{fq} = R_f i_{fq} + L_f \frac{d}{dt} i_{fq} + W_r L_f i_{fd} - V_{Gq} \tag{42}$$

$$\dot{i}_{fd} = \frac{1}{L_f} \left(-R_f i_{fd} + v_{fd} + W_r L_f i_{fq} + V_{Gd} \right) \tag{43}$$

$$\dot{i}_{fq} = \frac{1}{L_f}\left(-R_f i_{fq} + v_{fq} - W_r L_f i_{fd} + V_{Gq}\right) \tag{44}$$

with V_{Gd}, V_{Gq} indicated the input voltage of the AC-DC converter in the direct and quadrature frame. The electric network components of voltage and current on the AC side for both the direct and quadrature frame are given by v_{fd}, v_{fq}, i_{fd} and i_{fq} respectively, while the L_f referred to the inductance of the system. The active and reactive power is expressed as:

$$P = V_{Gd} i_{fd} + V_{Gq} i_{fq} \tag{45}$$

$$Q = V_{Gq} i_{fq} - V_{Gd} i_{fd}. \tag{46}$$

Remark 2. *Through setting the power factor to be 1 and neglecting the filter losses one can get the following expression* $V_{Gd} = V_{fd} = V_G, V_{Gq} = V_{fq} = 0$, *leading the active and reactive power to be* $P_f = V_G i_{fd}$ *and* $Q_f = -V_G i_{fq}$.

5. Nonlinear grid side converter model

Referring to Remark 2 we know that through setting the power factor to unity we get $V_{Gd} = V_{fd} = V_G, V_{Gq} = V_{fq} = 0$. In such a case the system is converted into single input-single output system in the form:

$$f(x) = \begin{pmatrix} -\dfrac{R_f}{L_f}x_1 + x_3 x_2 \\[2mm] -\dfrac{R_f}{L_f}x_2 - x_3 x_1 \\[2mm] -\dfrac{f_r}{J}x_3 - \dfrac{p}{J}\phi_{rd}x_2 \end{pmatrix}, \quad g(x) = \begin{pmatrix} \dfrac{2}{L_f} \\[2mm] 0 \\[1mm] 0 \end{pmatrix} \tag{47}$$

$$y = x_1. \tag{48}$$

where x: state vector $= \begin{bmatrix} i_{fd} & i_{fq} & W_r \end{bmatrix}^T$ $U = \begin{bmatrix} u_1 & u_2 \end{bmatrix}^T$.

5.1 Nonlinear modeling and control of the quadratic axis control

In this part, the asymptotic output tracking technique will be studied in the quadratic axis frame. The system has a well define the relative degree of $r = 1$. Consequently one can apply a coordinate transformation in the form $\Gamma(x) = \begin{pmatrix} x_1 \\ x_3 \\ x_2 \end{pmatrix}$.

The state space description in the new coordinates

$$\begin{cases} \dot{z}_1 = a(z,\eta) + b(z,\eta) \\[2mm] \dot{\eta}_1 = \dfrac{f_r}{J}\eta_1 - \dfrac{p}{J}\phi_{rd}\eta_2 \\[2mm] \dot{\eta}_2 = -\dfrac{R_f}{L_f}\eta_1 - \eta_2 z_1. \end{cases} \tag{49}$$

Remark 3. *The system has a stable zero dynamics. In fact by calculating the Jacobian matrix Q which describes the linear approximation at $\eta = 0$ of the zero dynamics of the original nonlinear system*

$$Q = \begin{pmatrix} \dfrac{f_r}{J} & -\dfrac{p}{J}\phi_{rd} \\ -\dfrac{R_f}{L_f}b & 0 \end{pmatrix} \tag{50}$$

we can see that the matrix is nonsingular. Hence the zero dynamics are asymptotically stable. The stability of the zero dynamics will depend on the parameters of the DFIG.

The stator of the DFIG was directly connected to the grid while its rotor was connected to it via a cascade (Rectifier, Inverter, and Filter). To evaluate the grid side model the power factor was set to one, thus only the quadratic rotor current will be produced. The voltage on the output of the inverter will suffer from disturbance signals formed by the original frequency $f = 50$ Hz and other signals. A passive R-L filter was used to eliminate harmonics. The input in the form $u = \frac{1}{a(z,\eta)}(-b(z,\eta) + c_0 z_1)$ ensures the reproduction of an output i_{rq} that will track the required reference signal. **Figure 5** depicts that the system nonlinear controller has reproduced an output that will converge asymptotically to the required reference signals and minimizes the effect of disturbance.

5.2 Feedback design under sampling

We now address the problem of preserving under system behavior under sampling. In fact, considering $u(t) \in U_T$ and $y(t) = y(kT)$ for $t \in [kT, (k+1)T]$ (T the sampling period). Now we compute the single-rate sampled data equivalent model of (43)

$$x_{k+1} = F^T(x_k, u_k) \tag{51}$$
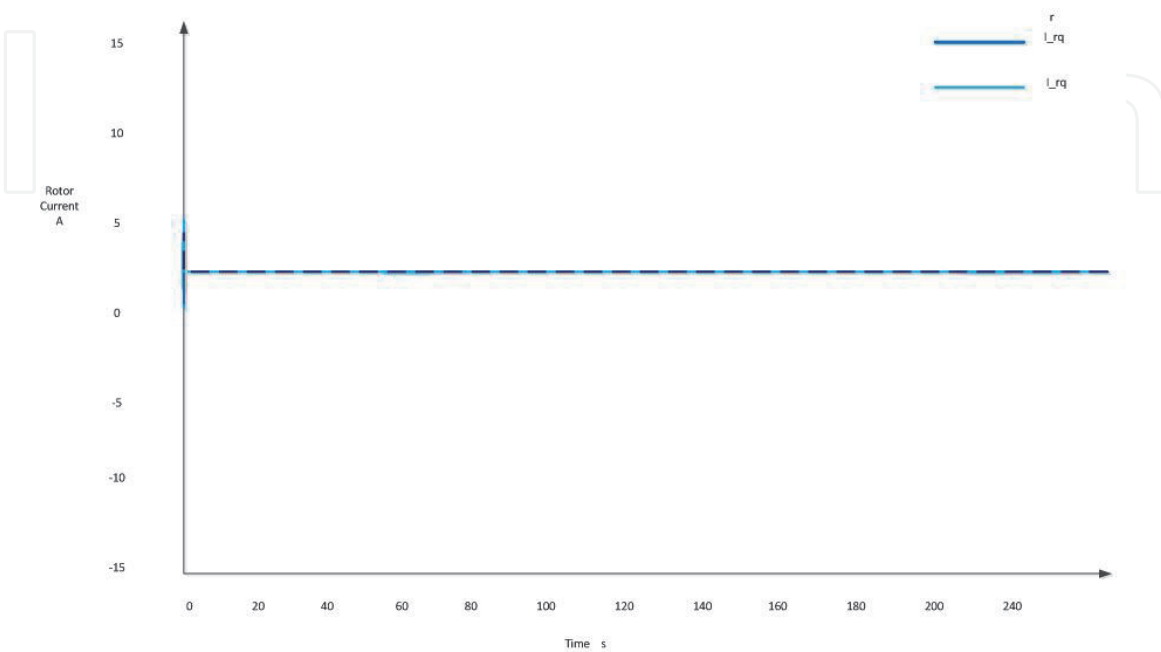
$$y_k = h(x_k) \tag{52}$$

Figure 5.
Nonlinear control applied to rotor current.

with $xk := x(kT), yk := y(kT), uk := u(kT), h(x) = i_{rd}$ and $F^T(xk, uk) = eT(Lf + ukLg)x_K$. In this case we compute a digital control law

$$u_d = u(kT) + Tw_{1k} \qquad (53)$$

which solve the problem.

5.3 Simulation

The wind speed and the DFIG are shown in **Figure 6**. The estimation of the wind speed was generated based upon the nonlinear mapping of the measured output power of the generator while taking into account the loss of power in the wind turbine. The quadratic rotor current that shall be set as the reference signal
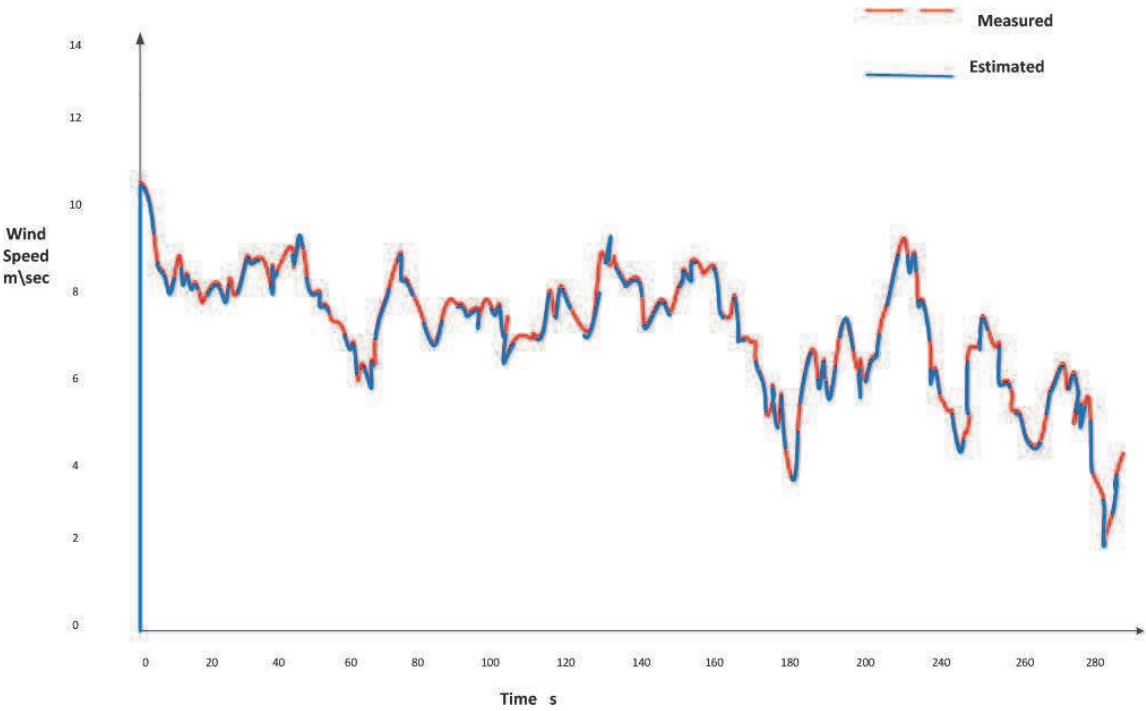
Figure 6.
Wind speed estimation.
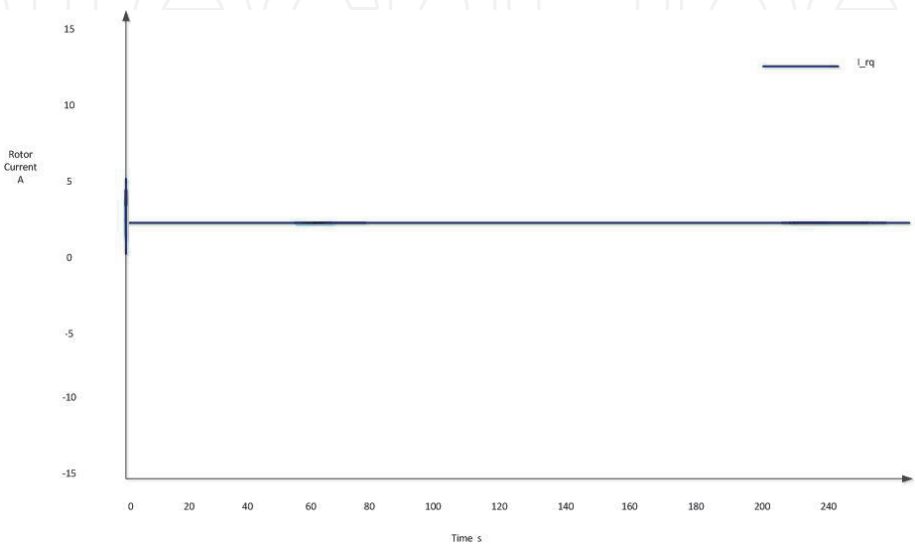
Figure 7.
DFIG rotor current.

so that a better performance is provided are shown in **Figure 7**. A feedback that is based on the proposed technique is applied and this will yield to an output signal that will follows the rotor signal (see **Figure 5**). **Figure 8** depicts the emulated and the sampled rotor speed after applying the feedback. Maximum Power Point Tracking technique was used to set the best conditions in order to arrive to maximum efficiency. It can be shown that sampled-data design provided better results such as the variation is smoother and the transient time is less than
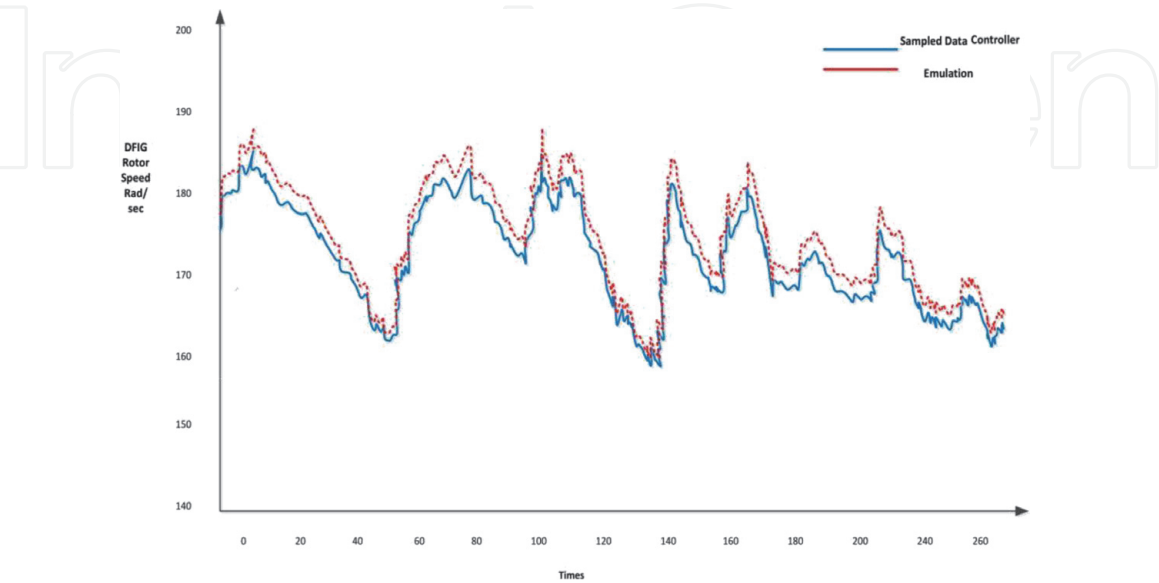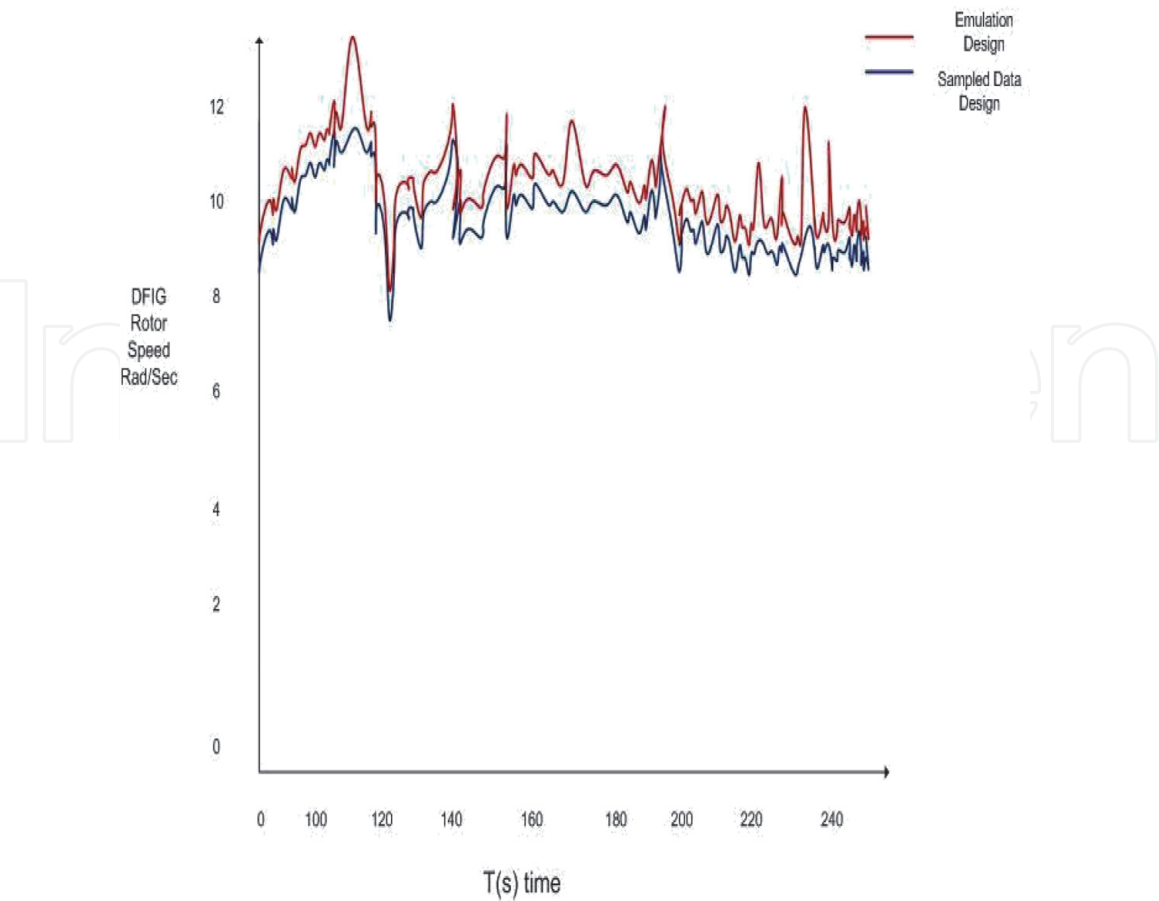

Figure 8.
DFIG rotor speed for MPPT.

Figure 9.
Tip speed ratio.

the emulated one. The **Tip Speed Ratio** TSR is illustrated in **Figure 9** for both the emulated and sampled base. The results will show that the TSR has been reduced by more than design which indicates that the size of power converters is reduced. Then, the power converters can be downsized without reducing the output power.

6. Conclusion

This paper aims to investigate the different modern control strategies in the power system application. In particular, the study will focus on the effect of nonlinear control techniques and SampledData Model when it is applied to a Doubly Fed Induction Generator DFIG. The mechanical model was first recalled and then the nonlinear model and control techniques were discussed. In the nonlinear, the asymptotic output tracking technique was chosen where feedback is designed to ensure that the system will converge to a specific target or reference. In this case, through controlling the direct and quadratic frame we can control the active and reactive power which was proven by the results. In the second half of the chapter we choose to investigate the digital control techniques where a comparison between the emulation design and the sampled data techniques are carried out The MATLAB program was to choose to simulate and test the control strategies. It can be noted from the results that as time increased the emulation design fail to preserve the same behavior as in the continuous-time and an oscillation takes place, unlike the sampled data design. Finally, it can be concluded that applying the sampled data model over the nonlinear system provides powerful results than the classical solution. Further investigation will be carried out regarding practical cases.

Acknowledgements

Author details

Marwa Hassan
Sapienza University of Rome, Rome, Italy

*Address all correspondence to: eng.marwaabdelhamied@gmail.com

References

[1] Intergovernmental Panel on Climate Change (IPCC). In: Edenhofer O, Pichs-Madruga R, Sokona Y, Seyboth K, Matschoss P, Kadner S, et al., editors. IPCC Special Report on Renewable Energy Sources and Climate Change Mitigation. Prepared by Working Group III of the Intergovernmental Panel on Climate Change. Cambridge University Press, Cambridge, United Kingdom/ New York, NY, USA; 2011. p. 1075. (Chapter 9)

[2] Turner JA. A realizable renewable energy future. Science. 1999;**285**(5428): 687-689

[3] Boyle G, editor. Renewable Energy. United Kingdom: Oxford University Press; 2004. p. 456. ISBN-10: 0199261784. ISBN-13: 9780199261789

[4] Wang F, Liu D, Zeng L. Modeling and simulation of optimal wind turbine configurations in wind farms. In: 2009 World Non-Grid-Connected Wind Power and Energy Conference. IEEE; 2009

[5] Wang F, Liu D, Zeng L. Study on computational grids in placement of wind turbines using genetic algorithm. In: 2009 World Non-Grid-Connected Wind Power and Energy Conference. IEEE; 2009

[6] Khare V, Nema S, Baredar P. Reliability analysis of hybrid renewable energy system by fault tree analysis. Energy & Environment. 2019;**30**(3): 542-555

[7] Iniyan S et al. Energy models for renewable energy utilization and to replace fossil fuels. Methodology. 2020;**67**:28-37

[8] Bauwens T, Devine-Wright P. Positive energies: An empirical study of community energy participation and attitudes to renewable energy. Energy Policy. 2018;**118**:612-625

[9] Niraula M et al. Variable stator frequency control of stand-alone DFIG with diode rectified output. In: 2018 5th International Symposium on Environment-Friendly Energies and Applications (EFEA). IEEE; 2018

[10] Kashkooli MRA, Madani SM, Lipo TA. Improved direct torque control for a DFIG under symmetrical voltage dip with transient flux damping. IEEE Transactions on Industrial Electronics. 2019;**47**:777-780

[11] Errouissi R et al. Offset-free direct power control of DFIG under continuous-time model predictive control. IEEE Transactions on Power Electronics. 2016;**32**(3):2265-2277

[12] Bektache A, Boukhezzar B. Nonlinear predictive control of a DFIG-based wind turbine for power capture optimization. International Journal of Electrical Power & Energy Systems. 2018;**101**:92-102

[13] Rashid G, Ali MH. Nonlinear control-based modified BFCL for LVRT capacity enhancement of DFIG-based wind farm. IEEE Transactions on Energy Conversion. 2016;**32**(1):284-295

[14] Li P et al. Nonlinear controller based on state feedback linearization for series-compensated DFIG-based wind power plants to mitigate sub-synchronous control interaction. International Transactions on Electrical Energy Systems. 2019;**29**:1

[15] Rashid G, Ali MH. Nonlinear control-based modified BFCL for LVRT capacity enhancement of DFIG-based wind farm. IEEE Transactions on Energy Conversion. 2016;**32**(1):284-295

[16] Yang B et al. Perturbation estimation based robust state feedback control for grid connected DFIG wind energy conversion system. International Journal of Hydrogen Energy. 2017; **42**(33):20994-21005

[17] Gao Y, Ai Q. Maximum power tracking control for parallel-operated DFIG based on fuzzy-PID controller. Journal of Electrical Engineering and Technology. 2017;**12**(6):2268-2277

[18] Ponce P, Ponce H, Molina A. Doubly fed induction generator (DFIG) wind turbine controlled by artificial organic networks. Soft Computing. 2018;**22**(9): 2867-2879

[19] Yogarathinam A, Chaudhuri NR. Wide-area damping control using multiple DFIG-based wind farms under stochastic data packet dropouts. IEEE Transactions on Smart Grid. 2016;**9**(4): 3383-3393

[20] Zhou Y et al. A dynamic weighted aggregation equivalent modeling approach for the DFIG wind farm considering the weibull distribution for fault analysis. IEEE Transactions on Industry Applications. 2019;**22**:1-7

[21] Zhou Y et al. A dynamic weighted aggregation equivalent modeling approach for the DFIG wind farm considering the Weibull distribution. In: 2019 IEEE/IAS 55th Industrial and Commercial Power Systems Technical Conference (ICPS). IEEE; 2019

[22] Nallappan G, Joo Y-H. Robust sampled-data fuzzy control for nonlinear systems and its applications: free-weight matrix method. IEEE Transactions on Fuzzy Systems. 2019; **27**:2130-2139